Coordination Environment of Copper Sites in Cu-CHA Zeolite Investigated by Electron Paramagnetic Resonance

Godiksen, Anita; Stappen, Frederick N.; Vennestrøm, Peter N. R.; Giordanino, Filippo; Rasmussen, Søren Birk; Lundegaard, Lars F.; Mossin, Susanne

Published in:
Journal of Physical Chemistry C

Link to article, DOI:
10.1021/jp5065616

Publication date:
2014

Document Version
Publisher's PDF, also known as Version of record

THE JOURNAL OF PHYSICAL CHEMISTRY C

Article

pubs.acs.org/JPCC

Coordination Environment of Copper Sites in Cu-CHA Zeolite Investigated by Electron Paramagnetic Resonance

Anita Godiksen,[†] Frederick N. Stappen,[†] Peter N. R. Vennestrøm,[‡] Filippo Giordanino,[§] Søren Birk Rasmussen,[‡] Lars F. Lundegaard,[‡] and Susanne Mossin*,[†]

[†]Centre for Catalysis and Sustainable Chemistry, Department of Chemistry, Technical University of Denmark, Lyngby, Denmark

[‡]Haldor Topsøe A/S, Nymøllevej 55, Lyngby, Denmark

[§]Department of Chemistry, NIS Centre of Excellence and INSTM Reference Center, University of Turin, Torino, Italy

ABSTRACT: Cu-CHA combines high activity for the selective catalytic reduction (SCR) reaction with better hydrothermal stability and selectivity compared to other copper-substituted zeolites. At the same time Cu-CHA offers an opportunity for unraveling the coordination environment of the copper centers since the zeolite framework is very simple with only one crystallographically independent tetrahedral site (T-site). In this study the results of an X-band electron paramagnetic resonance (EPR) investigation of ion-exchanged Cu-CHA zeolite with a Si/Al ratio of 14 ± 1 is presented. Different dehydration treatments and rehydration experiments are performed in situ while monitoring with EPR. The results are compared with recent literature evidence from temperature-programmed reduction, X-ray methods, IR spectroscopic methods, and UV−visible spectroscopy. On the basis of these findings quantitative information is obtained for the different copper positions in dehydrated Cu-CHA. The well-defined copper sites in the six-membered ring of the CHA structure are found to be EPR active, to give two distinct sets of signals in an approximate 1:1 ratio, and to add up to 19 ± 2% of the total copper in the material. The long-standing question of the EPR silent monomeric Cu^{2+} in copper-substituted zeolites is suggested to be copper species with an approximate trigonal coordination sphere appearing during the dehydration. After complete dehydration at 250 °C the majority of the EPR silent Cu^{2+} is suggested to exist as Cu^{2+}−OH^- coordinated to two framework oxygen atoms located in the microenvironment of an isolated Al T-site.

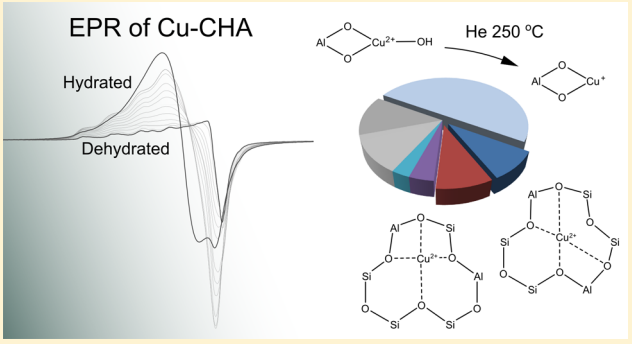

INTRODUCTION

Copper-exchanged zeolites have been characterized by a multitude of spectroscopic methods over the years. The initial fundamental investigations were followed by intense activity in the 1990s when copper zeolites were investigated as catalysts for the direct decomposition of NO into O_2 and N_2 and other deNOx reactions.[1] More recently Cu-MFI has attracted attention due to its activity in the partial oxidation of methane to methanol.[2,3] In the abatement of environmentally harmful nitrogen oxides, catalysts based on Cu-CHA have recently attracted extensive interest for the development of catalysts not based on vanadia for the selective catalytic reduction of nitrogen oxide using ammonia (NH_3-SCR) for mobile applications. Cu-SSZ-13 and Cu-SAPO-34, both with the CHA framework topology, are highly active as catalysts and have proven to be superior with respect to activity combined with hydrothermal stability of the zeolite material.[4−7] The recent commercialization of Cu-CHA for diesel engine exhaust treatment has sparked a high activity in this research field, but the identity and activity of the copper species and a rigorous mapping of the complexes present in the catalytic cycle have not yet been obtained. Recent progress includes several in situ studies.[8−10]

Electron paramagnetic resonance (EPR) has been used for the characterization of copper-exchanged zeolites since the 1970s. Single-crystal studies by EPR of natural chabazites substituted with Cu^{2+} were investigated by Lunsford in 1973.[11] A number of fundamental investigations by Larry Kevan in the 1980s[12] included different zeolite systems and other cations in the zeolites. The early investigations primarily focused on very low exchange ratios (<0.5%) in order to obtain well-resolved EPR spectra, but higher exchange ratios were also investigated for potential catalytic applications.[13] Copper in oxidation state +2 has one unpaired electron, and as for other Kramer's doublets it is usually possible to obtain an EPR spectrum using X-band EPR. By double integration of the EPR signal it is furthermore possible to quantify the EPR active copper. Information about the coordination environment can be extracted from the *g*-values and the hyperfine coupling constants for the interaction between the unpaired electron and the copper nucleus. Comprehensive literature of EPR investigations of small-molecule model systems and metal-

Received: July 1, 2014
Revised: September 8, 2014
Published: September 10, 2014

loproteins is available for comparison of parameter values.[14,15] At higher concentrations the paramagnetic centers interact giving rise to line broadening, and the resolution of the EPR spectrum decreases. If the copper centers are only connected by one atom, as in μ-oxo dimers, the two copper centers can interact antiferromagnetically or ferromagnetically depending on the bridging angle.[16]

During dehydration of certain copper zeolites most of the EPR signal disappears. This is the case for copper-exchanged zeolites with relatively high Si/Al ratios (e.g., >10) and high exchange ratios (close to Cu/Al = 0.5).[13,17,18] LoJacono et al. observed 55% of the signal disappearing from Cu-MFI by vacuum treatment at room temperature.[19] By heating, the effect starts below 100 °C and takes place when the dehydration is performed under vacuum, under static conditions or in a dry gas flow. For these materials typically about 50−80% of the signal is lost already at 200 °C. Several effects will result in the absence of the typical $S = 1/2$ EPR signal for copper. The suggestions may be summarized as

- *Reduction:* Copper in oxidation state +1 is diamagnetic, so any reduction of the copper center will result in the signal disappearing. Auto reduction of the copper centers has been shown by IR investigations to be relevant for copper-exchanged zeolites when heating in an inert atmosphere or under vacuum.[20]
- *Antiferromagnetic or ferromagnetic interactions*: In the case of close proximity of copper centers or an atom bridging the two copper centers, such as a μ-oxo or a μ-hydroxo dimer, the two unpaired electrons will commonly couple antiferromagnetically. This gives a diamagnetic singlet ground state and a higher lying triplet state. In materials with single oxide bridges the interaction is normally very strong (several hundred wavenumbers), and only the ground state singlet is occupied at ambient temperatures resulting in the dimeric or polymeric species being EPR silent. Similarly, if a paramagnetic copper center is coordinated directly to another paramagnetic center, such as an OH or NO radical, antiferromagnetic coupling between the two paramagnetic centers can cause the EPR signal to disappear. Less commonly, copper dimers with acute Cu−X−Cu angles can have ferromagnetic interactions (X is a bridging atom).[21] The resulting $S = 1$ ground state has a significantly different EPR spectrum.[22]
- *Pseudo Jahn−Teller effect (PJTE)*: When Cu^{2+} is forced into a coordination sphere which has a near-degenerate ground state the electronic degeneracy and a vibronic degeneracy (a vibronic double-well) can result in an E⊗e problem.[23] The coupling between the EPR transition and the vibration can broaden the electronic transitions in the EPR spectrum to such an extent that the signals corresponding to these monomeric Cu^{2+} species are difficult to observe even at low temperatures. The spin−lattice relaxation due to the very close lying excited state can become so fast at higher temperatures that it causes the signal to be completely absent.[24]

When Cu-CHA is heated in an oxygen-containing atmosphere, it is observed by IR using CO as a probe that only a negligible portion of the copper is reduced.[20,8] Therefore, the first point cannot be the sole explanation. A specific μ-oxo dimer is identified in Cu-MFI constituting only a minor amount of the copper in a sample with Si/Al = 12 and Cu/Al = 0.1−0.6 after activation in oxygen at >500 °C.[3] Cu^{2+} dimers are likely to be present at other activation temperatures and for other zeolites as well and to be related to the local aluminum distribution. If copper oxide phases or nanoparticles are generated during the dehydration or calcination, they will also be EPR silent. This is thought to be relevant for a varying percentage of the copper present after dehydration for all Cu zeolites—also for Cu-CHA, vide infra. It is very unlikely, however, to be the reason for 50% of the EPR signal of copper to disappear after room temperature vacuum treatment or dehydration temperatures below 100 °C. It is also not reasonable to suggest that non-Cu radicals such as OH or O_2^-[17] are formed in large amounts under such mild conditions. Indeed XANES data following the dehydration show that below 200° all copper is in oxidation state +2 with progressively lower coordination numbers depending on the dehydration temperature.[8,9] Therefore, we also discard the non-Cu radicals to be the main reason for the loss of EPR signal at low temperatures.

In conclusion the first two explanations are discarded for a large percentage of the Cu species in Cu-CHA dehydrated in an oxygen-containing gas at low temperatures, and we suggest that the third option is relevant for the Cu-CHA material and indeed for all overexchanged Cu zeolites. Conesa et al.,[13] LoJacono et al.,[19] Kucherov et al.,[25] Palomino et al.,[18] and Soria et al.[26] discuss that copper(II) in low-symmetry or trigonal-type sites could appear by dehydration and that it would be EPR silent. Conesa et al.[13] and Soria et al.[26] refer to work by Kazanskii et al.[27,28] and invoke the near-degeneracy of the electronic states as a reason for the EPR signal to be broadened beyond detection. The effect referred to is indeed the pseudo Jahn−Teller effect (PJTE)[23] and is distinguished from the more well-known proper Jahn−Teller effect by being active for systems not having high symmetry and a true degenerate ground state. A near-degenerate ground state is sufficient to influence the spectroscopic properties such as the observable EPR spectrum. In this work the EPR spectra of Cu-CHA are monitored under gentle dehydration in different gas streams, and an in situ method for exposing the dehydrated materials to traces of water is presented. On the basis of these experiments different Cu phases can be distinguished based on their EPR spectra and their response to traces of water. The phases can be quantified reproducibly with an uncertainty of a few percent relative to the total copper content. The results are compared to IR, UV−vis, and XRD data obtained on the same batch of Cu-CHA material after dehydration in a He/O_2 atmosphere, and suggestions to the identity of all of the different Cu phases are presented.

EXPERIMENTAL SECTION

Cu-CHA (Cu-SSZ-13), Cu-MFI (Cu-ZSM-5), and Cu-*BEA (Cu-Beta) were synthesized as described in ref 20, and the samples used in the present work are from the same batches as reported there. The Si/Al ratios are 14 ± 1 for Cu-CHA (Cu-SSZ-13), 11 ± 1 for Cu-MFI, and 13 ± 1 for Cu-*BEA. The samples were carefully calcined and rehydrated for several days at ambient conditions before the experiments. EPR signals assignable to carbon residues from template or organic counterions were not observed in the samples indicating that the calcinations were sufficient to remove them completely.[25,29]

Ex Situ. An amount of 10−20 mg of Cu zeolite sample was dehydrated in a dry (P_2O_5 dried) flow of oxygen in helium (50%) in a low-pressure-vacuum (LPV) quartz EPR tube by leading the gas (10 mL/min) through a loose capillary insert. The temperature was ramped to the dehydration temperature at 5−7 K/min and kept at the indicated temperature for 1.5−2 h. Then the capillary insert was lifted above the sample, and the gas flow was increased while the temperature was quickly

dx.doi.org/10.1021/jp5065616 | J. Phys. Chem. C 2014, 118, 23126−23138

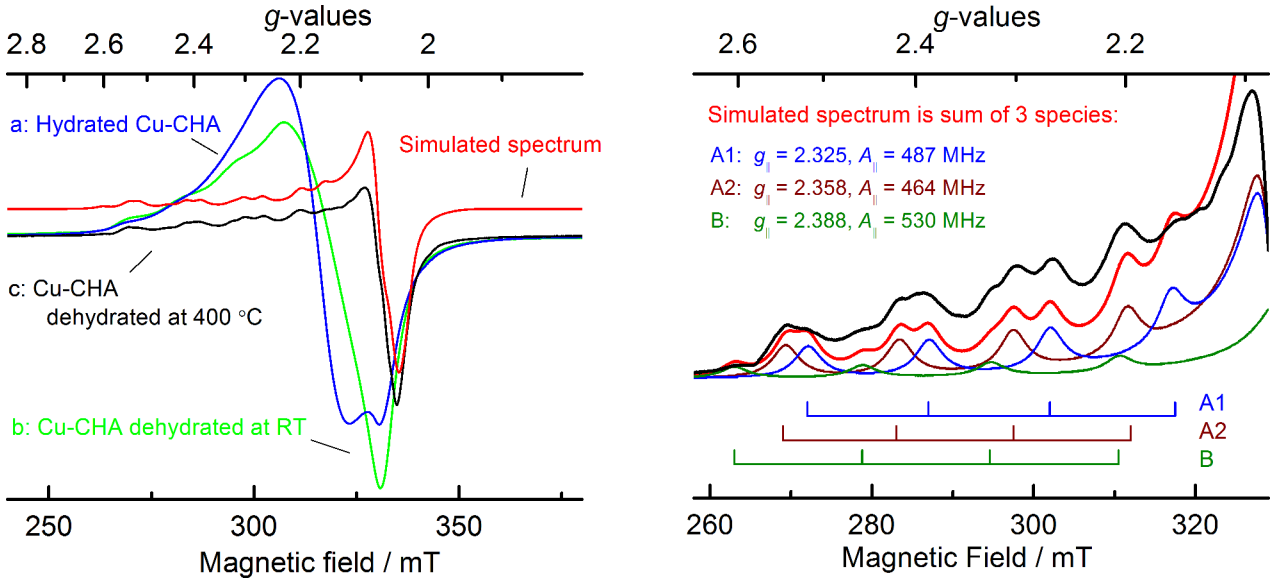

Figure 1. Left: Experimental EPR spectra of Cu-CHA recorded at room temperature. (a) Hydrated (blue), (b) dehydrated ex situ at room temperature under helium flow (green), and (c) dehydrated at 400 °C ex situ in an O_2/He flow (black). Spectrum (c) was simulated (red) using the spin Hamiltonian given in the main text and the parameters in Table 1. It is shifted on the *y*-axis to allow for comparison. Right: The low-field part of the experimental and simulated spectrum of Cu-CHA dehydrated at 400 °C is shown in greater detail. The simulation is the sum of the three different species A1 (blue), A2 (dark red), and B (dark green). The positions of the set of four parallel hyperfine peaks of the simulated spectrum of each species are marked.

decreased to RT. The flow was changed to pure He for approximately 2 min at RT to remove paramagnetic O_2 from the atmosphere in the tube. The capillary was removed while flowing, and the LPV tube was closed. The samples used in this work were never subjected to vacuum.

EPR spectra were collected with a continuous wave X-band Bruker EMX EPR spectrometer with the ER 4102ST cavity with a gunn diode microwave source in the field interval 220−400 mT. Ex situ spectra were collected with microwave power 6.3 mW, modulation frequency 100 kHz, modulation amplitude 8 G, frequency 9.3−9.7 GHz, and 4096 points and averaged over 10 sweeps. Tube and tube position in the cavity were kept constant. A background spectrum of the empty tube was collected before each experiment. All spectra shown have been corrected by subtracting the background spectrum from the experimental spectrum in each point. No other data correction was made. The background corrected spectra were integrated twice using the in-built facility in Origin 9.0 to compare the relative intensity. The spectra were simulated using the program WEPR95 by F. Neese[30] as a randomly oriented powder. Hyperfine coupling to $^{63/65}$Cu was treated as a perturbation, and the difference between the two isotopes was not resolved and therefore not taken into account. The line shape was Lorentzian for all simulated spectra. Quantification experiments of the hydrated catalyst (not shown) were performed relative to known copper(II) sulfate solid solutions in potassium sulfate.

In Situ. Cu-CHA was pressed to a pellet at 1 bar and sieved to 150−300 μm. An amount of 15−25 mg of sample was immobilized between two quartz wool plugs in a quartz tube with an inner diameter of 4 mm. Two independent gas manifolds with Bronkhorst mass flow controllers were fitted with stainless steel tubing to a four-way valve just outside the magnet of the EPR spectrometer. Switching between the two gas streams took effect at the site of the sample within seconds of turning the valve. The setup was tested for pressure drop each time. The reactant gas flow was kept at 100 mL/min. The gases were passed through a moisture trap (Supelco 5A Moisture Trap, 200 Cc with Swagelock Fittings) before entering the reactor during dehydration. The sample was heated using preheated atmospheric air with a Bruker EMX VT unit. The EPR spectra were measured continuously during the experiment with fast sweeps between 220 and 400 mT, microwave power 6.3 mW, modulation frequency 100 kHz, modulation amplitude 8 G, frequency 9.3−9.7 GHz, and 1024 points. Each spectrum took about 10 s to measure, and the field was swept to the start value for an additional 5 s giving a time resolution in the measurement of about 15 s.

RESULTS AND DISCUSSION

Ex Situ Dehydration. Representative spectra of Cu-CHA in the fully hydrated state and dehydrated at 400 °C are shown in Figure 1. All EPR spectra in Figure 1 were obtained at room temperature (RT). The total Cu content can be estimated by comparing these spectra with EPR calibration spectra obtained on samples containing varying amounts of $CuSO_4$ diluted in K_2SO_4, and good agreement is found with the concentration obtained from inductively coupled plasma optical emission spectroscopy (ICP-OES). This observation is also reported in the literature for EPR investigations of hydrated Cu-zeolites.[25,31] As shown in the preliminary EPR work presented by Giordanino et al.[20] the hydrated Cu-CHA has two negative peaks at g = 2.09 and at g = 2.14 in full accordance with Gao et al.[32] When performing the dehydration with a dry helium flow at RT for 14 h the g = 2.14 negative peak shifts to the 2.09 position, and slight hyperfine features appear in the low-field part of the spectrum. This is interpreted as the Cu^{2+} EPR spectrum coming from two different sites in the hydrated zeolite: (1) An isotropic spectrum from hydrated copper centers that have enough free movement to rotate or at least to change the elongation axis freely. (2) An anisotropic spectrum from copper centers that are restricted, probably due to the

exchange of a water ligand for a framework oxygen. After the gentle dehydration the majority of the water present on all surfaces is gone, and the isotropic copper species loses the freedom and also becomes anisotropic. 95% of the copper remains EPR active after this treatment, but reproducibly, 5% of the EPR signal is lost.

When dehydrating at higher temperatures much of the intensity is lost. After dehydration at 250 °C the signal intensity is only 25% of the intensity of the original hydrated sample. When performing the dehydration at 400 °C in an O_2/He flow the percentage is 33%. At 250 °C removal of water from the structure is complete according to in situ FT-IR and XAS, and the results after heating to higher temperatures depend on the dehydration atmosphere.[8] The intensity of the EPR spectrum of Cu-CHA is plotted as a function of the dehydration temperature in Figure 2. For comparison, values for Cu-MFI

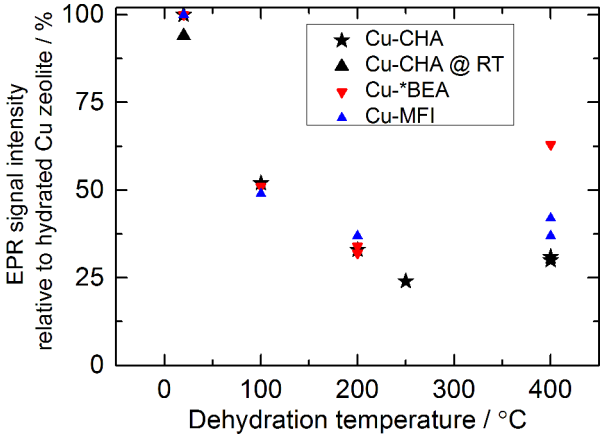

Figure 2. Total intensity of the EPR signal, calculated as a double integral, of the samples after ex situ dehydration at the given temperature for Cu-CHA (black stars), Cu-*BEA (red triangles), and Cu-MFI (blue triangles). The black triangle shows the 14 h room-temperature dehydration of CHA shown in green in Figure 1 (left). The EPR intensity is given in % relative to the value for the hydrated spectrum for each sample. Each point corresponds to one dehydration experiment. Multiple experiments performed on the same batch of material are plotted at some temperatures.

and Cu-*BEA with similar Si/Al and Cu/Al ratios are plotted in the same figure. All the copper zeolite materials follow the same trend at dehydration temperatures until 200 °C but differ after activation at higher temperatures. As was also described in ref 20 Cu-*BEA regains much of the intensity by heating to 400 °C, and Cu-MFI also regains more than Cu-CHA. The decrease in the double integral of the EPR signal after dehydration of Cu zeolites was also observed by LoJacono et al.,[19] Larsen et al.,[17,33] and Soria et al.[26] when starting from the hydrated zeolites. Kucherov et al.[34] did not observe such a dramatic decrease in the intensity when investigating samples which were carefully pretreated in an oxygen atmosphere at high temperatures before the EPR investigation. The increase of the signal intensity at higher dehydration temperatures was also previously observed as a slight increase for Cu-MFI[19,33] and as an even more pronounced regain of signal for Cu−Y.[13]

After ex situ dehydration at 400 °C and helium flush at room temperature three different copper species with well-resolved EPR spectra became visible for Cu-CHA (see Figure 1). The individual spectra were simulated using a simple axial spin Hamiltonian, eq 1, with $S = 1/2$ and $I = 3/2$[35]

$$H = g_{\|}\mu_B S_z B_z + g_{\|}\mu_B(S_x B_x + S_y B_y) + A_{\|} S_z I_z + A_{\perp}(S_x I_x + S_y I_y) \quad (1)$$

and averaged over a random distribution of crystallites. The simulated spectrum is the result of simple addition of three simulated spectra weighted as given in Table 1. The spin

Table 1. Speciation of Copper and Spin Hamiltonian Parameters of Species in One Representative Experiment of Cu-CHA Dehydrated Ex Situ at 400 °C (See Figure 1, Right)[a]

	spin Hamiltonian parameters			
	$g_{\|}$	$g_{\perp}$	$A_{\|}$	intensity relative to hydrated spectrum
A1	2.325	2.07	487 MHz	11%
A2	2.358	2.07	464 MHz	10%
B	2.388	2.07	530 MHz	5%
C	∼2.17	∼2.17	not resolved	∼7%
EPR silent	-	-	-	67%

[a] $A_{\perp}$ is not resolved in the spectra and is therefore not well determined; the value was set to 20 MHz in the simulated spectra. The amount of the isotropic species C is estimated from the difference between the double integral of the simulated and the experimental spectrum. The g-value is estimated as the zero-crossing of the spectrum obtained by subtracting the simulated spectrum from the experimental.

Hamiltonian parameters of the three different species are also given in Table 1. The line width parameters of all three species are assumed to be equal. After checking the result of a descent in symmetry in the spin Hamiltonian model, the model was kept axial in order to avoid overparameterization since the resolution in the perpendicular part of the spectrum was not high enough to justify a lower symmetry.

Besides the well-defined crystalline sites that are giving the sets of parallel peaks in Figure 1 (right), another phase must be present. An EPR line is shifting all the peaks up in the low-field part of the spectrum and down in the high-field part. If the sum of the simulated spectra is subtracted in every point from the experimental spectrum, the difference spectrum is reminiscent of a broad featureless isotropic Cu^{2+} EPR spectrum centered at $g = 2.17$. It integrates up to about 7% of the intensity of the original hydrated Cu-CHA and has been denoted site C in Table 1. The total intensity of the EPR spectrum of this Cu-CHA sample after dehydration adds up to 33% relative to the hydrated sample. Since the spectra of the hydrated and dehydrated samples are all collected at RT, it is not necessary to take the Boltzmann distribution into account, and the values given in Table 1 can be translated directly to the amount of EPR-active Cu^{2+} species in the sample after dehydration. At least five different copper species are present in the sample after dehydration at this temperature according to EPR.

The relative amount of the different species is sample and preparation dependent, and other Cu-CHA samples with other Si/Al and Cu/Al ratios are expected to give different values. For Cu-MFI and Cu-*BEA different amounts of EPR silent Cu species were observed as well as different A- and g-values for the EPR active Cu species.

In Situ Dehydration and Rehydration. Cu-CHA was dehydrated in O_2/He at 250 °C for 2 h, returned to RT under the same atmosphere, and then exposed to a pure helium gas

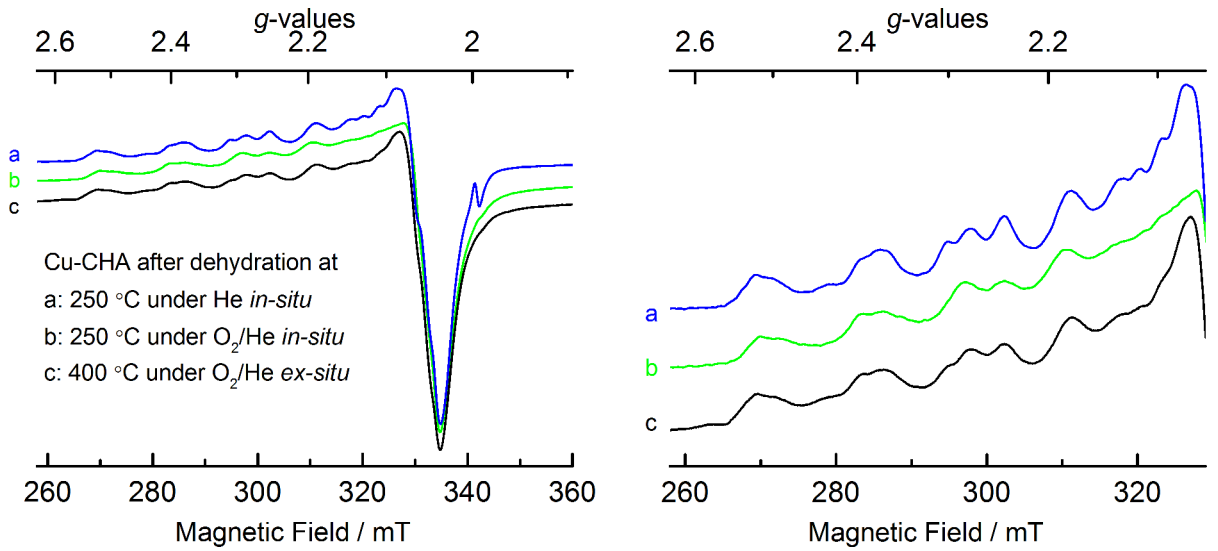

Figure 3. Comparison of EPR spectra of Cu-CHA after different dehydration methods. All spectra are collected at RT. (a) and (c) Are collected under He atmosphere, and (b) is collected under an O_2/He atmosphere. The small peak at $g = 2.0$ in spectrum (a) was identified as coming from the thermocouple which had entered the cavity of the EPR instrument slightly in this particular experiment. The signal is not from the sample. A zoom-in of the same spectra is shown on the right.

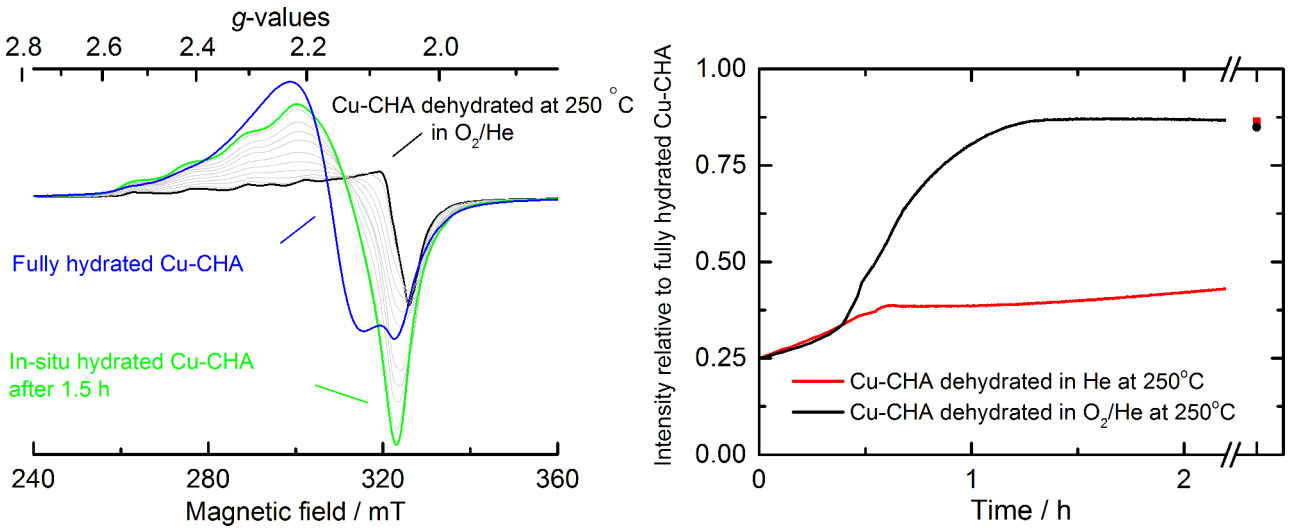

Figure 4. Left: In-situ EPR spectra of Cu-CHA after dehydration at 250 °C in an O_2/He flow (black line) and successive spectra during the slow exposure to trace water at RT. The anisotropic spectrum after 1.5 h is outlined in green, and the final spectrum after exposure to moist ambient conditions without flow for several days is shown in blue. Right: The development with time of the double integral (the intensity) of the EPR spectra of dehydrated Cu-CHA during controlled exposure to moisture is shown. The black line corresponds to the sample initially dehydrated in an O_2/He flow at 250 °C. The red line shows the corresponding results after dehydration at 250 °C in a pure helium flow.

(99.95%) stream directly from the flask without the use of a moisture trap mounted before the EPR cell. The spectrum right after cooling (still under O_2/He) is shown in Figure 3. The features are the same as in the sample dehydrated in an O_2/He flow ex situ at 400 °C, but the interaction with the paramagnetic oxygen broadens the features and marginally shifts the hyperline lines. The total intensity of the EPR spectrum is 25% of the fully hydrated sample in accordance with the ex situ experiment at 250 °C but lower than the ex situ experiment performed at 400 °C (see Figure 2). The flow was changed to He with the temperature maintained at RT. The time-resolved spectra during the exposure to the insufficiently dried He gas are shown in the left part of Figure 4. The negative peak of the EPR spectrum shifts quickly to lower fields as was found in the anisotropic part of the hydrated spectrum in Figure 1. Gradually a broad but still anisotropic spectrum appears during a period of a few hours, and the double integral increases. The overall features of the spectrum do not change after the first minutes, and the resulting spectrum is essentially the same as for dehydration at room temperature (see the green trace in Figure 1). The spectrum is predominantly anisotropic which indicates that the establishment of a hydration shell with full rotational freedom of certain copper sites does not occur completely under relatively dry flow conditions. The black trace in the right part of Figure 4 shows the development in the intensity at RT during exposure to the pure He flow. The intensity increases continuously and reaches a plateau corresponding to 87% of the intensity of the original hydrated spectrum before dehydration. When the sample is allowed to equilibrate with the atmosphere *without* a gas flow the original

Table 2. Quantification and EPR Activity of the Species Present in Cu-CHA after in Situ Dehydration at 250 °C in O_2/He and in Pure He[a]

site	dehydrated in O_2/He (2 h)	dehydrated in He (14 h)	EPR signal after dehydration (reason if not[b])	EPR signal after trace H_2O exposure	EPR signal after trace H_2O/O_2 exposure	assignment	number of close Al per Cu
A1	9%	9%	yes	yes	yes	Cu^{2+} in 6mr	2
A2	9%	9%	yes	yes	yes	Cu^{2+} in 6mr	2
B	4%[c]	4%	yes	yes	yes	5 coord. Cu^{2+}	2
C	3%[c]	3%	yes	yes	yes	Cu^{2+} in noncryst. 2 Al sites	2
D	12%[d]	13%	no (AF coupling)	yes	yes	"reactive Cu_xO_y"	1
E	50%[d]	-	no (PJTE)	yes	yes	Cu^{2+}-OH^-	1
F	-	50%	no (diamagnetic)	no	yes	Cu^+	1
G	13%	12%	no (AF coupling)	no	no	Cu oxide clusters	0−1

[a]The results are determined using the method described in the text. The assignments are tentative based on the arguments described below. The uncertainties are estimated to be ±2 on the percentages given. [b]AF = antiferromagnetic, PJTE = pseudo Jahn−Teller effect. [c]Sites B and C cannot be distinguished in the experiment with O_2/He dehydration alone due to lower resolution. [d]Sites D and E cannot be distinguished in the experiment with O_2/He dehydration alone. The distribution of 50% and 12% is therefore based on the He dehydration experiment as well.

spectrum with both anisotropic and isotropic features and ∼100% intensity is regained after a few days.

The experiment was repeated with dehydration in pure helium flow at 250 °C for 14 h. The EPR spectrum recorded right after cooling is given in trace a in Figure 3. The spectrum after dehydration in He was identical to the spectrum of the sample dehydrated in an O_2/He flow at 400 °C (see Figure 3) and almost identical to the sample dehydrated in an O_2/He flow at 250 °C (apart from the higher resolution). The intensity is 25% relative to the fully hydrated starting point. The red trace in the right part of Figure 4 gives the development in the intensity at RT during exposure to the untreated He flow. The initial development in the intensity of the EPR spectrum was the same as for the sample dehydrated in the O_2/He mixture; this time, however, the total intensity of the spectrum stabilizes at 38%. After several hours the sample was exposed slowly also to traces of O_2. After this treatment the intensity and the spectrum converge to the spectrum obtained in the in situ experiment performed after the O_2/He dehydration (green spectrum in Figure 4, left). The intensity is marked in Figure 4 (right) as a single red dot.

Finally, the flow was stopped, and the sample was exposed to moist ambient conditions. The signal intensity slowly increased from 87% to ∼100% after several days, and the spectrum again became similar to the blue spectrum in Figure 4 regardless of the dehydration conditions that the sample was exposed to.

EPR signals assignable to an $S = 1$ multiplet from magnetically coupled copper dimers were not observed at any time in either experiment.

A summary of the results is shown in Table 2 where the Cu sites are grouped according to the EPR response when using the in situ exposure to traces of water. The majority of the Cu species that become EPR silent in the O_2/He dehydration is not reduced since the EPR signal may be recovered just by exposure to trace amounts of H_2O. Any deviations in the copper species present after the two different dehydration treatments are therefore present *only* in the percentage of the copper which is EPR silent. This is a very informative result: the Cu species that are autoreduced after 14 h in the He flow at 250 °C therefore belong exclusively to the percentage of Cu which is EPR silent after dehydration.

Assignment of Cu Species in Cu-CHA That Are EPR Active after Dehydration. When the Cu-CHA sample is dehydrated under in situ flow conditions at 250 °C and cooled quickly to room temperature (RT) and traces of H_2O are avoided by the use of a moisture trap, only 25% of the copper is EPR active. The EPR active A1, A2, B, and C sites are distinguishable as reported in Table 2, and the suggestions for assignments below are based upon information from the EPR spectra in combination with other spectroscopic information.

Sites A1 (9%) and A2 (9%) give essentially the same EPR spectra after the 400 °C ex situ dehydration and after the 250 °C in situ dehydrations (see Figure 3). The amounts of A1 and A2 integrate up to approximately the same percentage of Cu. They are assigned to Cu^{2+} residing in well-defined positions in the six-membered ring (6mr) sites with two aluminum T-sites. This is based on the following arguments:

(a) The EPR parameters of both sites correspond to a 4O tetragonal coordination mode for Cu^{2+}, vide infra.
(b) The quantification by EPR and by XRD[36] measured on the same Cu-CHA zeolite exposed to similar dehydration conditions has the same percentage, ∼20%, of the copper in the 2Al 6mr sites.
(c) As shown in Figure 3, these sites are not reduced at 250 °C in a helium flow. The EPR spectrum of these sites only disappears when reducing the sample in a pure helium flow at 400 °C or higher temperatures (not shown) or when using a reducing gas. This is in correspondence with these sites being expected to be less reducible when H_2O is not present.[9]
(d) No species with exactly these set of EPR parameters were found in EPR spectra of dehydrated Cu-MFI and Cu-*BEA, and these do not possess similar 6mr units.
(e) A plausible explanation can be given for the existence of two separate Cu^{2+} sites in a 6mr with 2 Al T-sites, vide infra.

When investigating dehydrated Cu-CHA by X-ray methods[36−39] the Cu site in the 6mr is consistently found. A 6mr containing 2 Al T-sites is sufficient to charge balance a bare Cu^{2+} ion and has been suggested in the literature to be the preferred site at low Cu loadings.[40] The plane of the 6mr sites provides a distorted tetragonal planar coordination environment for Cu^{2+}. Cu^{2+} is likely to induce small distortions since the framework is flexible to a certain extent, and the oxygen atoms are further away than what is usually preferred for Cu^{2+}.[39,41] Since the two aluminum atoms counterbalancing the charge of the Cu^{2+} ion in the 6mr cannot be adjacent due to

Löwenstein's rule and because the six T-sites are related by symmetry, two options are possible (see Chart 1). The two options correspond to having the two Al tetrahedrons located diagonally across the 6mr or only separated by one Si tetrahedron. Without considering the effects of distorting the framework, it is expected that the sites, where copper binds to the maximum amount of aluminum-bound oxygens, will be more stable since these oxygens carry most of the negative charge. This leads to only one preferred position of Cu^{2+} for each of the two Al sitings in the 6mr.[41]

Chart 1. Possible Cu^{2+} Sitings in 2 Al 6mr Sites with Two Al and Four Si T-Sites in CHA[a]

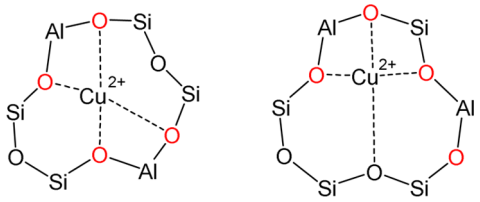

[a]Oxygens directly bound to aluminum are marked in red. Only the possibilities with Cu^{2+} coordinated to the maximum number of oxygens bound to aluminum are given.

The two spin Hamiltonian parameters $g_{||}$ and $A_{||}$ have been related to the copper coordination environment in a number of copper containing proteins and simple coordination compounds.[14,15] The values found here for A1 and A2 correspond well to Cu^{2+} in a tetragonal planar arrangement with four oxygen donors. The framework atoms provide a rigid frame, where the strong T−O bonds and preference of the framework T-sites to have tetrahedral coordination have priority over the weaker coordination bonds to copper.[42] Since the two sites have slightly different spin Hamiltonian parameters, we can attempt an assignment to the structures in Chart 1. The structure to the right in Chart 1 is calculated by DFT to have three short Cu−O bonds and one which is significantly longer.[41] The structure on the left has four short Cu−O bonds. The unpaired electron on copper is in the d_{x2-y2} orbital pointing directly at the ligands (see Figure 5). The negative charge of oxygen is felt more strongly by the unpaired electron in A1 than in A2. A more negative coordination environment will result in a lower $g_{||}$ and a higher $A_{||}$ value.[43] A plausible assignment is therefore that site A1 from the EPR spectrum in Figure 1 corresponds to the structure pictured on the left in Chart 1, and site A2 corresponds to the structure pictured on the right.

Site B (4%): The spin Hamiltonian parameters for site B are close to the values for hydrated copper zeolites measured at cryogenic temperatures which are assigned to 5- or 6-coordinate sites.[44,45] Site B is therefore assigned to a very small amount (<5%) of well-defined copper sites that have tetragonal 5-coordination (square pyramidal). These are not immediately identifiable in an idealized completely dehydrated CHA structure, but it might be that some well-defined sites have scavenged trace water during the measurement at RT despite using high purity helium and an additional moisture trap or that a small percentage of well-defined but nonideal CHA sites are present. The resolution was not high enough to assess this site in the in situ experiment with O_2/He in Figure 3.

Site C (3%) has an unresolved broad EPR spectrum. It is assigned to isolated Cu^{2+} in noncrystalline 2 Al sites. These could be related to the extra-framework aluminum, which is known to be present in almost all synthesized zeolites[8] or near structural defects in the zeolites.

Assignment of Species in Cu-CHA That Are EPR Inactive after Dehydration. The EPR quantification in Table 2 suggests that we have so far only accounted for 25% of the copper after the dehydration at 250 °C. Sites D, E, F, and G in Table 2 are all EPR inactive after the dehydration, but the signal is regained after different treatments. This allows us to distinguish between the EPR silent species below.

Site D (12%) consists of a relatively small amount of EPR silent copper that was not reduced during the He treatment but

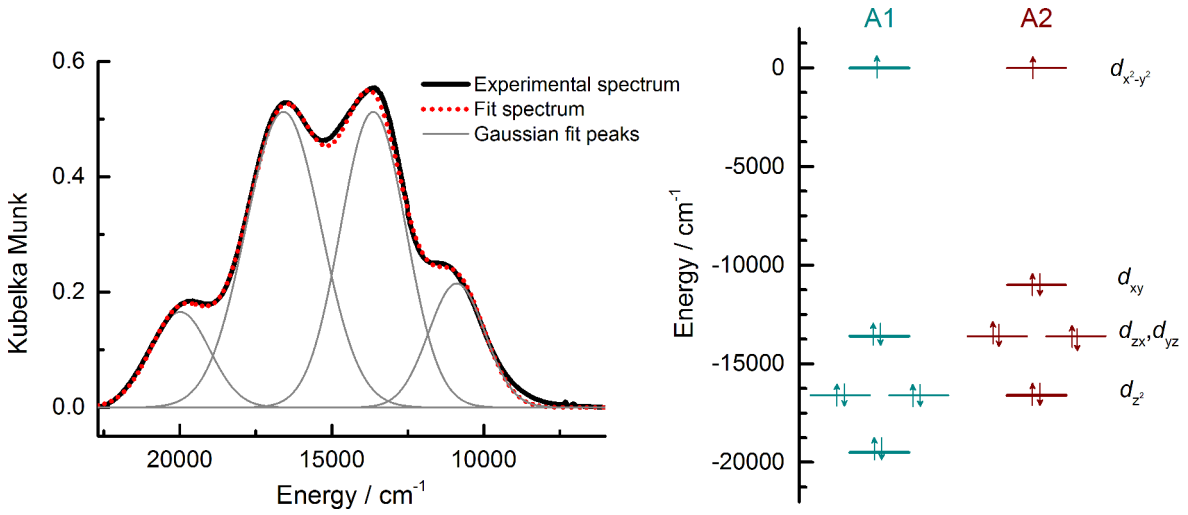

Figure 5. Left: Experimental values from UV−vis[20] and a fit to four Gaussian functions. The band positions found are 20 000; 16 600; 13 600 and 10 900 cm^{-1} and the relative intensities are 1.0:4.0:3.5:1.2 (in the same order). Right: The energy diagram of the d-orbitals for the assignment of the d-d transitions to two separate tetragonal Cu^{2+} sites. The energy of $d_{x^2-y^2}$ is shifted to 0. It is assumed that each site has approximate degeneracies of the d_{zx} and d_{yz} orbitals. The resulting separate three-line spectra for A1 and A2 have an accidental overlap giving the observed four bands in the experimental spectrum. The energies of the d-d transitions (the energy differences between $d_{x^2-y^2}$ and the other four d-orbitals) are listed in Table 3.

dx.doi.org/10.1021/jp5065616 | J. Phys. Chem. C 2014, 118, 23126−23138

easily undergoes hydrolysis and becomes EPR active when the sample is exposed to traces of water. Verma et al. suggest the presence of $Cu^{2+}-O-Cu^{2+}$ dimers in an 8mr with 2 Al in Cu-CHA activated in oxygen.[46] If present, these sites would belong to site D. Due to antiferromagnetic coupling between the two Cu^{2+} centers, $Cu^{2+}-O-Cu^{2+}$ sites are EPR silent at room temperature, and $Cu^{2+}-O-Cu^{2+}$ species in zeolites are known to be very susceptible to traces of water.[3] The same would be true for other small copper oligomers as well, which is why we have tentatively named this species as "reactive Cu_xO_y". After hydrolysis the bridge is broken, and two $Cu^{2+}-OH^-$ monomers are produced. If exposed to even more water they will become EPR active like the other $Cu^{2+}-OH^-$ species, vide infra. During the He dehydration at relatively low temperature the bridging extra-framework oxygen atom is expected to protect the Cu^{2+} centers toward autoreduction. The material investigated by Verma et al. has a lower Si/Al ratio of 4.5 and will have a higher density of Cu sites at comparable Cu/Al ratios compared to the material investigated here with Si/Al = 14 ± 1. The percentage of dimers is therefore expected to be lower in the material investigated in this work.

We tentatively assign site D to consist of $Cu^{2+}-O-Cu^{2+}$ dimers and other small oligomers that are reactive toward water: "reactive Cu_xO_y". We recognize that any $Cu^{2+}-OH^-$ species that fail to be reduced after 14 h in the He flow would also be included in this site, and if any EPR Cu^{2+} in 2 Al sites are present (such as trigonal bipyramidal Cu^{2+}) they would also belong to this site. The evidence presented here therefore only gives an upper limit of 12% of the total amount of Cu belonging to these species and should not be considered as a positive identification of a "$Cu^{2+}-O-Cu^{2+}$" site.

Site E (50%): The presence of $Cu^{2+}-OH^-$ sites has been suggested before.[13,25,33] Recently spectroscopic evidence of $Cu^{2+}-OH^-$ sites emerged based on an IR band of $Cu^{2+}-OH^-$ at 3657 cm^{-1}.[20] DFT calculations[36] indicate that Cu^{2+} is coordinated to two framework oxygens and one OH^- group in an approximately planar coordination environment. Such a species is argued to be EPR silent due to the PJTE, vide infra. After exposure to traces of water at RT in an inert atmosphere it will again become EPR active: the water molecules can supplement the coordination shell until, ultimately, a tetragonal Cu^{2+} EPR spectrum reappears. We assign site E to be $Cu^{2+}-OH^-$ coordinated to two framework oxygen atoms bound to a single Al T-site.

Site F: Dehydration in inert gas is known to result in partial reduction of Cu^{2+}; the so-called "autoreduction".[20] Our results corroborate this since the EPR spectrum of site F is not regained after exposure to traces of water. In the O_2/He dehydrated sample, which is known to be reduced only to a negligible amount,[8,20] a much higher percentage of the signal is regained when exposed to traces of H_2O. Thus, the difference in EPR intensity between pretreatment in He and in O_2/He (Figure 4, right) is assigned to reduction that has taken place at 250 °C after 14 h in the pure He flow. Therefore, we assign site F to be Cu^+ probably bound to two framework oxygen atoms from a 1 Al site.[36]

Site G (13%): The EPR signal of these sites is not regained even by exposure to traces of both water and oxygen. The percentage of copper in this site is the same after both dehydration methods (see Figure 4). Only exposure to ambient conditions for several days without a flow allows these species to become EPR active again. The copper in site G is assigned to noncrystalline polynuclear copper oxide clusters and sub-nanoparticles present in the material formed when copper is caught with too few charge-compensating Al centers in the vicinity during dehydration.[47] This species needs a full hydration film and possibly also access to oxygen before it dissolves and disperses to give EPR active fully hydrated tetragonal Cu^{2+} monomers.

Assignment of Bands from A1 and A2 in the UV−vis Spectrum of Dehydrated Cu-CHA. UV−vis spectroscopy performed on the same Cu-CHA sample before and after dehydration at 400 °C in an O_2/He atmosphere is reported by Giordanino et al.[20] Four unprecedented sharp bands are observed in the d−d region of the UV−vis spectrum, which is reproduced in Figure 5, and a dark blue color is observed for dehydrated Cu-CHA compared to the pale green color for Cu-MFI and Cu-*BEA.[20] Contributions from the minor sites B and C are expected to be typical weak and featureless tetragonal Cu^{2+} signals. Since they sum up to only ∼7% this contribution is expected be too modest to identify. As outlined below, the UV−vis spectrum of the dominant site E is expected to be severely broadened compared to tetragonal Cu^{2+} signals at RT or above. Sites D, F, and G are not expected to give identifiable d−d transitions in this region since they are not assigned to monomeric Cu^{2+}. This leaves A1 and A2 which, unlike all the other sites, have very well-defined and stiff coordination environments provided entirely by framework atoms. Since the strong covalent bonds of the framework dictate the Cu coordination environment; it is not possible to maintain an inversion center in the coordination sphere of Cu in A1 or A2 as is otherwise usually observed for tetragonal Cu^{2+}. Therefore, the Laporte selection rule is relaxed, and more intense UV−vis bands than normal are expected for these distorted tetragonal Cu^{2+} sites. A Gaussian fit of the four bands (see Figure 5 left) provides transitions at 20 000, 16 600, 13 600, and 10 900 cm^{-1}. The relative integrated intensity is 1.0:4.0:3.5:1.2 (in the same order). The orbital energy diagram for a d^9 electron configuration is shown for an almost tetragonal Cu^{2+} system in the right part of Figure 5. Square planar Cu^{2+} (D_{4h}) is well characterized in model systems, and a typical pattern of the absorption spectrum is three bands with energy differences of 3000 cm^{-1} and the center band corresponding to transitions to the E (D_{4h}) level being more intense than the other two.[48] The lower symmetry of sites A1 and A2, while important for increasing the intensity, is not expected to split the E (D_{4h}) level severely: E (D_{4h}) is only split by the *difference* in π-donor strength along the x compared to the y direction, and similar ligands are present at comparable distances to Cu. Therefore, the analogy is maintained to square planar model systems such as $CuCl_4^{2-}$, and the assignment is performed analogously.[48] The values of the assignment are also in correspondence with calculated values for tetragonal Cu^{2+} in a zeolite environment.[49] Awaiting a dedicated DFT computational study of the UV−vis spectrum of these sites, the four UV−vis bands in Figure 5 are tentatively assigned to the A1 and A2 sites found by EPR, the four bands resulting from two sets of three bands overlapping. Using the arguments given under the assignment of the sites observed in EPR, a more negative and therefore stronger average ligand field was assumed for A1. Therefore, the set of three bands with higher energies is assigned to A1. The assignment is summarized in Table 3.

In order to assess whether this assignment of the experimental UV−vis spectrum is reasonable, ligand field theory parametrized using the angular overlap model (AOM) was applied.[50] Only the ^2D multiplet is taken into account in

Table 3. Assignment of Transition Energies of Species A1 and A2 to the Four Lines in the Experimental UV−Vis Spectrum in the Left Part of Figure 5[a]

	A1	A2
$d_{x^2-y^2}$	0	0
d_{xy}	13 600 cm^{-1}	10 900 cm^{-1}
d_{zx}	16 600 cm^{-1}	13 600 cm^{-1}
d_{yz}	16 600 cm^{-1}	13 600 cm^{-1}
d_{z^2}	20 000 cm^{-1}	16 600 cm^{-1}

[a]The d orbital diagrams for each site with this assignment are shown in the right part of Figure 5. d_{zx} and d_{yz} are not expected to be completely degenerate, but since the energy difference is not resolved in the spectrum, they have been assigned the same value.

the AOM model, but there are still too many parameters in the model to determine from only three observed bands for each site. A number of simplifying assumptions about the symmetry have therefore been made. d orbitals are gerade, and a model limited to the ^2D multiplet cannot detect the loss of the inversion center. We assume that the angular deviations are minor and force 90° angles and an inversion center on the model. The σ-donor and π-donor strength of each of the four ligands are thus projected upon a planar orthorhombic model (D_{2h}) giving *trans*-$Cu(L_1)_2(L_2)_2$ for site A1 and *trans*-$Cu(L_3)_2(L_4)_2$ for site A2. Each pair of averaged ligands L_n (n = 1−4) has a σ-donor parameter, e_σ, and π-donor parameter, e_π, in this model. This ligand model was used to fit the two sets of experimental values assigned in Table 3 with the Ligfield computer program by J. Bendix.[51,52] The result is the following sets of AOM parameters

$$\text{A1: } e_\sigma(L_1) = 7500\ cm^{-1},\ e_\pi(L_1) = 1700\ cm^{-1},\ e_\sigma(L_2) = 5700\ cm^{-1},\ e_\pi(L_2) = 0\ cm^{-1}$$

$$\text{A2: } e_\sigma(L_3) = 5500\ cm^{-1},\ e_\pi(L_3) = 1500\ cm^{-1},\ e_\sigma(L_4) = 5500\ cm^{-1},\ e_\pi(L_4) = 0\ cm^{-1}$$

The parameters are reasonable since oxygen donor ligands such as water and hydroxide are reported to have e_σ = 7900 cm^{-1} and e_π = 1500 cm^{-1}.[53] The ligands that are further away from the copper center are expected to have lower σ-donor strength and much lower π-donor strength. This is corroborated by the model results. We conclude that the assignment in Table 3 has resulted in a reasonable set of AOM parameters. Obviously a substantial error bar is likely present for all band positions and fitted parameters. It was attempted to correlate the EPR parameters and the energies obtained from UV−vis bands in the same way as given in ref 49, but the test of whether the covalency could be decoupled failed in this case.

In conclusion the AOM model with a series of assumptions qualitatively agrees to the assignment of the observed four bands in the UV−vis spectrum to originate as a superposition of two spectra originating from coordination environments like the A1 and A2 sites depicted in Chart 1.

Pseudo Jahn−Teller Effect of a Three-Coordinate Cu^{2+}−OH^- Site. Andersen et al.[36] suggest based on DFT calculations that the monomeric three-coordinate Cu^{2+}−OH^- site is related to environments with a single Al framework atom with an acute angle of ∼80° for O−Cu−O. The O−Cu−OH angle is calculated to be ∼137° for the most favored Cu^{2+}−OH^- 1 Al site (in the 8mr) and ∼130° for the second most favored (in the 6mr).[54] In order to investigate this Cu^{2+} coordination environment qualitatively a d-orbital diagram was calculated using the AOM model. The O−Cu−O angle was fixed at 80°, and the energies of the 5 d-orbitals were calculated as a function of the O−Cu−OH angle (see Figure 6)

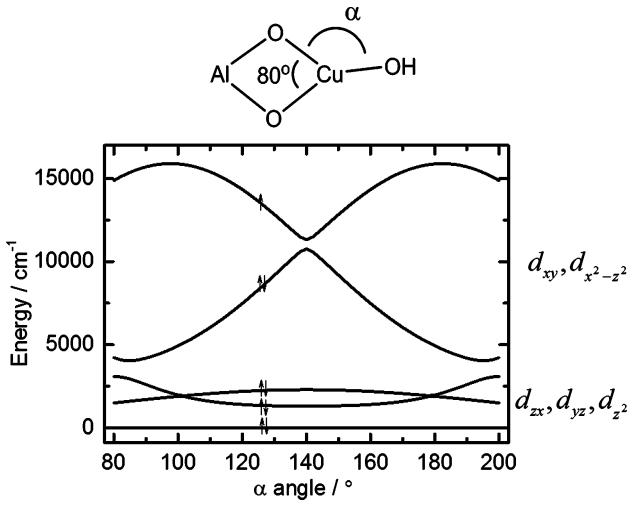

Figure 6. Top: Planar three-coordination calculated by DFT.[36] Bottom: d-orbital energies are plotted as a function of the O−Cu−OH angle (Walsh diagram) for an angle between 80 and 200°. Energies of the five d orbitals are calculated using Ligfield.[51] The AOM parameters of all three oxygen donor ligands are assumed to be e_σ = 7500 cm^{-1} and e_π = 1700 cm^{-1}. The d orbital with the lowest energy is shifted to zero. The energies of the d−d transitions in this d^9 system can be obtained from the diagram by calculating the energy difference between the d orbital with the highest energy and one of the other four, compared to the energy scale in Figure 5 (right).

(Walsh plot). The AOM parameters obtained for the strongest set of ligands in the 6mr copper species above were used for all three ligands since they are expected to settle at the shortest bonds possible with only three ligands available: $e_\sigma(L)$ = 7500 cm^{-1}, $e_\pi(L)$ = 1700 cm^{-1}. A hypothetical truly trigonal d^9 system with 120° angles will have an electronically degenerate E (D_{3h}) ground state. The d-orbitals in the plane of the ligands (d_{xy} and $d_{x^2-y^2}$) have the highest energy. Lowering the symmetry to C_{2v} having one 80° and two 140° angles, corresponding to the middle position in Figure 6 (bottom), the electronical degeneracy of the ground state is lifted, but the energy difference between d_{xy} and $d_{x^2-y^2}$ is only a few hundred cm^{-1}.

The Jahn−Teller theorem[55,56] states that the ground state of a d^9 system cannot be degenerate, and some distortion of the bonds will take place in order to relieve a degeneracy resulting from high symmetry. The symmetry of the framework-bound Cu^{2+}−OH^- species is not high enough to invoke the Jahn−Teller theorem. Even a near-degeneracy of the ground state influences the spectroscopic properties, however, and the PJTE[57] has been found to be important for many Kramer's systems.[23] Cu^{2+} in a planar three-coordinate coordination sphere with three similar ligands is an obvious candidate to have a strong PJTE. A stringent treatment of this particular geometry for Cu^{2+} is to our knowledge not found in the literature and is beyond the scope of this work. The following discussion will therefore be qualitative. The bonds to the two framework oxygen donors are rigid, but the hydroxide group bound to Cu has more freedom to change. The softest vibration around copper is therefore expected to be the specific

bend vibration corresponding to the change of the α angle in Figure 6. The adiabatic potential energy surface (APES) corresponding to this vibration has two minima: one on each side of the central 140° angle. The coupling between the electronic degeneracy (E) and the vibronic degeneracy (e), E⊗e, can be detrimental for observing electronic transitions,[23] the effect being called the E⊗e problem. The microwave energy absorbed during an EPR transition is dissipated through spin−lattice vibrations. If the relaxation is almost as fast or faster than the time scale of EPR (9.5 GHz for X-band EPR), the excited state will be able to relax before it is detected, and the EPR spectrum is broadened or not observable at all.[24] In this case the unpaired electron is in a d orbital in the plane of all the coordinating atoms. A pathway for fast relaxation of the excited electronic spin state is presumably present for all of the temperatures tested since: (1) The energy of the half-filled orbital is highly influenced by the position of a group involved in a soft bend vibration. 2) There is a low-lying excited state only a few hundred cm^{-1} away. (3) The coupling is allowed by symmetry. The relaxation is tentatively suggested to be due to a Raman (vibration) relaxation process at higher temperatures and, possibly, a tunneling process at very low temperatures since the APES is symmetric.[56] It was attempted to detect the signal by collecting an EPR spectrum at 4 K of Cu-CHA activated in O_2/He at 400 °C in an EPR tube, which was exposed shortly to a mild vacuum at RT and sealed off. Even this was not a sufficiently low temperature to provide a discernible EPR signal from any of the missing Cu^{2+} species in the EPR spectrum. The EPR signal started disappearing at dehydration conditions below 100 °C for all the measured Cu-zeolites in this work (see Figure 2), and similar observations have also been made by vacuum treatment at RT on Cu-MFI.[19] The maximum amount of the three-coordinate species depicted in the top of Figure 6 probably only appears after full dehydration above 220 °C.[8,9] The symmetry arguments made above are valid for any approximately trigonal species with the strong donor ligands in the plane. The EPR signal is also suggested to be broadened or even disappear for a trigonal bipyramidal or an approximately tetrahedral geometry around copper obtained as an intermediate in the dehydration process. It is energetically favored to have all the strong donor ligands in the equatorial plane around Cu^{2+} since the SOMO is then destabilized and the fully occupied orbitals are stabilized. Hydroxide and the partially negative framework oxygens are stronger donors than water and will occupy positions in the plane. As soon as the fourth ligand in the equatorial plane is lost during dehydration, the EPR spectrum is speculated to also disappear.

The PJTE is also expected to have an impact on the larger energy scale of UV−vis transitions. The slope of the energy of the singly occupied molecular orbital (SOMO) with respect to the α angle is large (see Figure 6, bottom). Vibrations changing this angle will change the energy of *all* the d−d bands of site E in the UV−vis spectrum since this orbital is involved in all transitions from the ground state. Therefore, we suggest that the unprecedented sharp d−d bands observed in the UV−vis spectrum cannot originate in site E. Since no other lines are immediately identifiable we suggest that the three-coordinate Cu^{2+}−OH^- sites are in fact not discernible in the spectrum even though 50% of the copper is suggested to belong to this site. UV−vis measurements of dehydrated Cu-CHA at cryogenic temperatures would reveal if vibrations in such a species can be frozen out. These investigations are still pending.

In conclusion we find that only EPR spectra assigned to tetragonal monomeric Cu^{2+} are observed. Three-coordinate Cu^{2+}−OH^- coordinated to two framework oxygens, most likely associated with the environment of a single Al site, is not expected to be observable at room temperature by EPR spectroscopy due to the PJTE.

Final Comments. The speciation and tentative assignments of the copper in the Cu-CHA sample based on the two dehydration−rehydration experiments are summarized in Table 2 and Figure 7. Peden et al. have earlier proposed two different

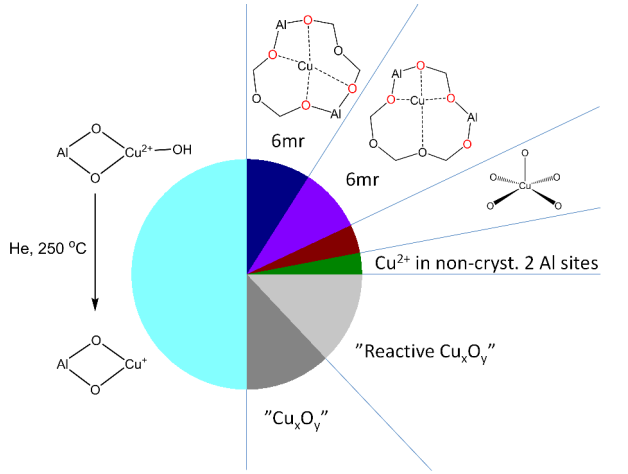

Figure 7. Speciation diagram of Cu-CHA after dehydration at 250 °C showing the assignment of different species discernible by EPR using the in situ dehydration−rehydration method described in the text. The results for the EPR active species are largely the same as for the ex situ dehydration at 400 °C in Table 1, except for the slightly lower total sum of EPR active species after the 250 °C dehydrations.

Cu sites in CHA-zeolites based on two different peaks in the H_2-TPR profile,[40] and this is directly corroborated by our results: Site E is easily autoreduced under our experimental conditions, whereas A1, A2, B, C, and D require higher temperatures or a reducing agent. Recent DRIFT measurements under reducing conditions point to the majority of the easily reducible copper to be situated in the 8mr.[9] The mechanism of the autoreduction is not fully known, and the EPR investigation is not able to resolve this since the transformation takes place between two EPR silent species. Larsen et al. suggest a mechanism involving a simple homolytic cleavage of the Cu−OH bond giving Cu^+ and an OH radical.[17] In support of this suggestion we argument that the 2 Al Cu sites A1 and A2 are suggested not to have this group and are not reduced at 250 °C in a flow of helium.

The quantification of Cu^{2+} in 2 Al 6mr sites can be compared with the statistics given in refs 46 and 58. We find 18−21% of the total Cu in 2 Al 6mr sites. Using the Cu/Al ratio of the sample of 0.44 we obtain a total Cu/Al ratio of Cu in 6mr sites to be ∼0.09. This is in excellent agreement with the prediction of the statistical model of 0.09 for a Si/Al ratio of 14.

Cu-MFI loses EPR signal to the same extent as Cu-CHA under the experimental conditions described here. The resulting EPR active species are less resolved after dehydration, and the line pattern is dissimilar to the ones in Cu-CHA. This is partially due to the much higher number of possible sites with slightly different geometries in a more complicated framework structure. A comparable speciation of the EPR active sites in MFI has not been performed yet. Palomino et al.[18] report that a

large percentage of EPR signal is lost during dehydration, and a portion of this is regained when the dehydrated Cu-MFI sample is exposed to deoxygenated water. Cu-MFI likely has a larger percentage of the "reactive Cu_xO_y" in the form of $Cu^{2+}-O-Cu^{2+}$ after dehydration in a dry oxygen stream judged by the prominent 22 700 cm^{-1} UV−vis line.[3] Any copper on isolated single Al sites is, if present, expected to be similar to the $Cu^{2+}-OH^-$ sites suggested for Cu-CHA here.

Cu-*BEA loses the same amount of EPR signal during dehydration as the other two Cu zeolites for dehydration temperatures below 250 °C (see Figure 2). At higher dehydration temperatures a significantly different overall EPR intensity profile is seen. A much larger percentage of the EPR silent copper becomes EPR active after dehydration at higher temperatures. We suggest that either the copper is able to migrate into EPR active sites, which most likely are 2 Al sites, and thereby eliminate water, or other factors such as internal structural defects play an important role. For Cu−Y with high Si/Al ratio almost all of the intensity is reported to come back,[13] and we have preliminary data corroborating this. These observations clearly indicate that the specific coordination environment for copper is dictated by the zeolite structure, and it is decisive for the reappearance of the EPR signal without coordination to any adsorbants.

CONCLUSIONS

Several characterization techniques have now been used on the same Cu-CHA material, and some of the most important findings of these investigations are the identification of the $Cu^{2+}-OH^-$ IR band and the 4-line UV−vis spectrum,[20] the electron density in the 6mr and in the 8mr from XRD and DFT,[36] and the detailed speciation of the sites based on EPR spectroscopy presented here. This allows for more confidence in the assignment of the copper sites. The highly symmetric CHA framework only provides a limited number of copper sites, and therefore EPR spectroscopy is able to characterize and quantify them directly (A1, A2, B, and C corresponding to isolated Cu^{2+} monomers in different tetragonal coordination environments) or indirectly (D, E, and F corresponding to "reactive Cu_xO_y", $Cu^{2+}-OH^-$, and Cu^+ sites) when using the in situ protocol outlined here. Some ambiguity is still possible in the assignment of the sites based on the EPR data, but overall quite restrictive boundaries have been placed on the amount of each of the different species present. The investigation by EPR is complementary to the other methods used so far: IR, UV−vis, EXAFS, XRD, etc. The different species present have been investigated even if present in only minor percentages of the total copper. The experiments are completely reproducible to within a few % when using the same batch of material.

Ligand field analysis of the UV−vis spectrum of the dehydrated sample is in accordance with the assignment of the A1 and A2 species to isolated Cu^{2+} sites in the 6mr described in a number of publications.[37,39] The PJTE is presented to explain the loss of EPR spectrum by dehydration of Cu-CHA when only one Al is available per Cu due to the vibrations of the charge-balancing OH^- group coupling to the electronic degeneracy of Cu^{2+}. It is suggested that it will be relevant for other Cu zeolites as well if they have too few 2 Al sites available for the amount of Cu^{2+} exchanged into the material. 1 Al sites with two oxygens facing a cavity or a larger channel in the framework are present in all zeolite materials with moderate to high Si/Al ratios to some extent. The low symmetry coordination environment for Cu^{2+} was put forth by some authors before to explain the loss of EPR signal, but the implications of the PJTE for Cu zeolites was not mentioned by the majority of the workers investigating these materials. The use of vacuum during dehydration or high temperature pretreatments, as well as the more complicated zeolite structures previously investigated, did not allow the detailed argumentation presented here, which is based on spectroscopically well-identified sites in a very simple zeolite structure. As seen in Table 2 and Figure 7, all the EPR active sites suggested after dehydration have 2 Al per Cu center, and all the EPR inactive sites have 1 or less Al per Cu. Therefore, we are working toward applying careful analysis of the EPR response of ion-exchanged copper as a complementary experimental tool to investigate 2 Al sites and the local framework in a range of zeotypes.

After being left at ambient conditions all investigated copper zeolites always revert to 100% EPR active fully oxidized and fully hydrated Cu^{2+}.

AUTHOR INFORMATION

Corresponding Author

*E-mail: slmo@kemi.dtu.dk. Tel.: +45 45252391.

Author Contributions

The manuscript was written through contributions of all authors. All authors have given approval to the final version of the manuscript.

Notes

The authors declare no competing financial interest.

ACKNOWLEDGMENTS

This work was financially supported by the Danish Independent Research Council DFF − 1335-00175 and DFF − 09-070250, Carlsbergfondet is acknowledged for supporting the upgrade of the EPR instrument at Department of Chemistry, DTU.

REFERENCES

(1) Iwamoto, M.; Furukawa, H.; Mine, Y.; Uemura, F.; Mikuriya, S.; Kagawa, S. Copper(II) Ion-Exchanged ZSM-5 Zeolites as Highly Active Catalysts for Direct and Continuous Decomposition of Nitrogen Monoxide. *J. Chem. Soc., Chem. Commun.* **1986**, 1272−1273.

(2) Alayon, E. M. C.; Nachtegaal, M.; Bodi, A.; van Bokhoven, J. A. Reaction Conditions of Methane-to-Methanol Conversion Affect the Structure of Active Copper Sites. *ACS Catal.* **2014**, *4*, 16−22.

(3) Woertink, J. S.; Smeets, P. J.; Groothaert, M. H.; Vance, M. A.; Sels, B. F.; Schoonheydt, R. A.; Solomon, E. I. A $[Cu_2O]^{2+}$ Core in Cu-ZSM-5, the Active Site in the Oxidation of Methane to Methanol. *Proc. Natl. Acad. Sci. U. S. A.* **2009**, *106*, 18908−18913.

(4) Kwak, J. H.; Tonkyn, R. G.; Kim, D. H.; Szanyi, J.; Tran, D.; Lee, J.; Peden, C. H. F. Excellent Activity and Selectivity of Cu-SSZ-13 in the Selective Catalytic Reduction of NOx with NH_3. *J. Catal.* **2010**, *275*, 187−190.

(5) Fickel, D. W.; D'Addio, E.; Lauterbach, J. A.; Lobo, R. F. The Ammonia Selective Catalytic Reduction Activity of Copper-Exchanged Small-Pore Zeolites. *Appl. Catal. B: Environ.* **2011**, *102*, 441−448.

(6) Deka, U.; Lezcano-Gonzalez, I. Local Environment and Nature of Cu Active Sites in Zeolite-Based Catalysts for the Selective Catalytic Reduction of NOx. *ACS Catal.* **2013**, *3*, 413−427.

(7) Gao, F.; Kwak, J. H.; Szanyi, J.; Peden, C. H. F. Current Understanding of Cu-Exchanged Chabazite Molecular Sieves for Use as Commercial Diesel Engine DeNOx Catalysts. *Top. Catal.* **2013**, *56*, 1441−1459.

(8) Giordanino, F.; Borfecchia, E.; Lomachenko, K. A.; Lazzarini, A.; Agostini, G.; Gallo, E.; Soldatov, A. V.; Beato, P.; Bordiga, S.; Lamberti, C. Interaction of NH3 with Cu-SSZ-13 Catalyst: A

Complementary FTIR, XANES and XES Study. *J. Phys. Chem. Lett.* **2014**, *5*, 1552−1559.
(9) Kwak, J. H.; Varga, T.; Peden, C. H. F.; Gao, F.; Hanson, J. C.; Szanyi, J. Following the Movement of Cu Ions in a SSZ-13 Zeolite during Dehydration, Reduction and Adsorption: A Combined in Situ TP-XRD, XANES/DRIFTS Study. *J. Catal.* **2014**, *314*, 83−93.
(10) Doronkin, D. E.; Casapu, M.; Gu, T.; Mu, O.; Frahm, R.; Grunwaldt, J.-D. Operando Spatially- and Time-Resolved XAS Study on Zeolite Catalysts for Selective Catalytic Reduction of NO_x by NH_3. *J. Phys. Chem. C* **2014**, *118*, 10204−10212.
(11) Chao, C.-C.; Lunsford, J. H. EPR Spectra of Cu^{2+} in Single Crystals of Chabazite. *J. Chem. Phys.* **1973**, *59*, 3920−3925.
(12) Narayana, M.; Kevan, L. Detection of a New Trigonal Bipyramidal Copper Species in Cu−CaX Zeolite by Electron Spin Resonance and Electron Spin Echo Modulation Analysis. *J. Chem. Phys.* **1983**, *78*, 3573−3578.
(13) Conesa, J. C.; Soria, J. Electron Spin Resonance of Undetected Copper(II) Ions in Y Zeolite. *J. Phys. Chem.* **1978**, *82*, 1847−1850.
(14) Peisach, J.; Blumberg, W. E. Structural Implications Derived from the Analysis of Electron Paramagnetic Resonance Spectra of Natural and Artificial Copper Proteins. *Arch. Biochem. Biophys.* **1974**, *165*, 691−708.
(15) Sakaguchi, U.; Addison, A. W. Spectroscopic and Redox Studies of Some copper(II) Complexes with Biomimetic Donor Atoms: Implications for Protein Copper Centres. *J. Chem. Soc., Dalton Trans.* **1979**, 600−608.
(16) Atanasov, M.; Angelov, S.; Mayer, I. Modelling of Angular Dependence of Superexchange: Application to Copper(II) Dimers. *J. Mol. Struct.* **1989**, *187*, 23−33.
(17) Larsen, S. C.; Aylor, A.; Bell, A. T.; Reimer, J. A. Electron Paramagnetic Resonance Studies of Copper Ion-Exchanged ZSM-5. *J. Phys. Chem.* **1994**, *98*, 11533−11540.
(18) Palomino, G. T.; Fisicaro, P.; Bordiga, S.; Zecchina, A.; Giuria, V.; Giamello, E.; Lamberti, C. Oxidation States of Copper Ions in ZSM-5 Zeolites. A Multitechnique Investigation. *J. Phys. Chem. B* **2000**, *104*, 4064−4073.
(19) LoJacono, M.; Fierro, G.; Dragone, R.; Feng, X.; D'Itri, J.; Hall, K. W. Zeolite Chemistry of CuZSM-5 Revisited. *J. Phys. Chem. B* **1997**, *101*, 1979−1984.
(20) Giordanino, F.; Vennestrøm, P. N. R.; Lundegaard, L. F.; Stappen, F. N.; Mossin, S.; Beato, P.; Bordiga, S.; Lamberti, C. Characterization of Cu-Exchanged SSZ-13: A Comparative FTIR, UV-Vis, and EPR Study with Cu-ZSM-5 and Cu-B with Similar Si/Al and Cu/Al Ratios. *Dalton Trans.* **2013**, *42*, 12741−12761.
(21) Atanasov, M.; Delley, B.; Reinen, D. A DFT Study of the Energetical and Structural Landscape of the Tetrahedral to Square-Planar Conversion of Tetrahalide Complexes of Copper(II). *Z. Anorg. Allg. Chem.* **2010**, *636*, 1740−1750.
(22) Chao, C.-C.; Lunsford, J. H. EPR Study of Copper(II) Ion Pairs in Y-Type Zeolites. *J. Chem. Phys.* **1972**, *57*, 2890−2898.
(23) Bersuker, I. B. Pseudo-Jahn-Teller Effect−a Two-State Paradigm in Formation, Deformation, and Transformation of Molecular Systems and Solids. *Chem. Rev.* **2013**, *113*, 1351−1390.
(24) Broser, I.; Schulz, M. Untersuchung der Breite der ESR Signale von C^{u2}+ in ZnO-Kristallen. *Z. Physik* **1972**, *254*, 35−45.
(25) Kucherov, A.; Karge, H.; Schlögl, R. Quantitative ESR Study of the CuH-ZSM-5 System: Influence of Preparation and Pretreatment Techniques on the Valence State of Copper. *Microporous Mesoporous Mater.* **1998**, *25*, 7−14.
(26) Soria, J.; Martinez-Arias, A.; Martinez-Chaparro, A.; Conesa, J. C.; Schay, Z. Influence of the Preparation Method, Outgassing Treatment, and Adsorption of NO And/or O_2 on the Cu^{2+} Species in Cu-ZSM-5: An EPR Study. *J. Catal.* **2000**, *190*, 352−363.
(27) Mikheikin, I. D.; Shvets, V. A.; Kazanskii, V. B. Sites of Copper Ion Localization in Type Y Zeolites Studied from Optical and EPR Spectra. *Kinet. Katal.* **1970**, *11*, 747−752.
(28) Kazanskii, V. B.; Mikheikin, I. D. Internal Report, Russian Academy of Science, Chemistry. *Izd. Otd. Khim. Nauk* **1973**, *6*, 361.
(29) Occhiuzzi, M.; Fierro, G.; Ferraris, G.; Moretti, G.; Chimica, D.; Universita, S.; Moro, P. A. Unusual Complete Reduction of Cu^{2+} Species in Cu-ZSM-5 Zeolites under Vacuum Treatment at High Temperature. *Chem. Mater.* **2012**, *24*, 2022−2031.
(30) Neese, F.; Zumft, W. G.; Antholine, W. E.; Kroneck, P. M. H. The Purple Mixed-Valence Cu A Center in Nitrous-Oxide Reductase: EPR of the Copper-63, Copper-65, and Both Copper-65 and [^{15}N] Histidine-Enriched Enzyme and a Molecular Orbital Interpretation. *J. Am. Chem. Soc.* **1996**, *118*, 8692−8699.
(31) Kucherov, A.; Gerlock, J.; Jen, H.; Shelef, M. In Situ Esr Monitoring of the Coordination and Oxidation States of Copper in Cu-ZSM-5 up to 500° C in Flowing Gas Mixtures: 1. Interaction with He, O_2, NO, NO_2, and H_2O. *Zeolites* **1995**, *15*, 9−14.
(32) Gao, F.; Walter, E. D.; Karp, E. M.; Luo, J.; Tonkyn, R. G.; Kwak, J. H.; Szanyi, J.; Peden, C. H. F. Structure−activity Relationships in NH3-SCR over Cu-SSZ-13 as Probed by Reaction Kinetics and EPR Studies. *J. Catal.* **2013**, *300*, 20−29.
(33) Carl, P. J.; Larsen, S. C. EPR Study of Copper-Exchanged Zeolites: Effects of Correlated G - and A -Strain, Si/Al Ratio, and Parent Zeolite. *J. Phys. Chem. B* **2000**, *104*, 6568−6575.
(34) Kucherov, A.; Gerlock, J. In-Situ Determination by ESR of the Oxidation State of Copper in Cu-ZSM-5 in Flowing He and O2 up to 500. Degree. C. *J. Phys. Chem.* **1994**, *98*, 4892−4894.
(35) Abragam, A.; Bleaney, B. *Electron Paramagnetic Resonance of Transition Ions*; Clarendon P.: Gloucestershire, 1970.
(36) Andersen, C. W.; Bremholm, M.; Vennestrøm, P. N. R.; Blichfeld, A. B.; Lundegaard, L. F.; Iversen, B. B. Location of Cu^{2+} in CHA Zeolite Investigated by X-Ray Diffraction Using the Rietveld/Maximum Entropy Method. *IUCrJ.* **2014**, DOI: 10.1107/S2052252514020181.
(37) Korhonen, S. T.; Fickel, D. W.; Lobo, R. F.; Weckhuysen, B. M.; Beale, A. M. Isolated Cu^{2+} Ions: Active Sites for Selective Catalytic Reduction of NO. *Chem. Commun.* **2011**, *47*, 800−802.
(38) Deka, U.; Eilertsen, E. A.; Emerich, H.; Green, M. A.; Korhonen, S. T.; Weckhuysen, B. M.; Beale, A. M. Confirmation of Isolated Cu^{2+} Ions in SSZ-13 Zeolite as Active Sites in NH_3-Selective Catalytic Reduction. *J. Phys. Chem. C* **2012**, *116*, 4809−4818.
(39) Fickel, D. W.; Lobo, R. F. Copper Coordination in Cu-SSZ-13 and Cu-SSZ-16 Investigated by Variable-Temperature XRD. *J. Phys. Chem. C* **2010**, *114*, 1633−1640.
(40) Kwak, J. H.; Zhu, H.; Lee, J. H.; Peden, C. H. F.; Szanyi, J. Two Different Cationic Positions in Cu-SSZ-13? *Chem. Commun.* **2012**, *48*, 4758−4760.
(41) Göltl, F.; Bulo, R. E.; Sautet, P. What Makes Copper-Exchanged SSZ-13 Zeolite Efficient at Cleaning Car Exhaust Gases? *J. Phys. Chem. Lett.* **2013**, *4*, 2244−2249.
(42) Comba, P.; Schiek, W. Fit and Misfit between Ligands and Metal Ions. *Coord. Chem. Rev.* **2003**, *239*, 21−29.
(43) Kivelson, D.; Neiman, R. ESR Studies on the Bonding in Copper Complexes. *J. Chem. Phys.* **1961**, *35*, 149−155.
(44) Pierloot, K.; Delabie, A.; Groothaert, M. H.; Schoonheydt, R. A. A Reinterpretation of the EPR Spectra of Cu(II) in Zeolites A, Y and ZK4, Based on Ab Initio Cluster Model Calculations. *Phys. Chem. Chem. Phys.* **2001**, *3*, 2174−2183.
(45) Groothaert, M. H.; Pierloot, K.; Delabie, A.; Schoonheydt, R. a. Identification of Cu(ii) Coordination Structures in Cu-ZSM-5, Based on a DFT/ab Initio Assignment of the EPR Spectra. *Phys. Chem. Chem. Phys.* **2003**, *5*, 2135−2144.
(46) Verma, A. A.; Bates, S. A.; Anggara, T.; Paolucci, C.; Parekh, A. A.; Kamasamudram, K.; Yezerets, A.; Miller, J. T.; Delgass, W. N.; Schneider, W. F.; et al. NO Oxidation: A Probe Reaction on Cu-SSZ-13. *J. Catal.* **2014**, *312*, 179−190.
(47) Wang, D.; Zhang, L.; Li, J.; Kamasamudram, K.; Epling, W. S. NH3-SCR over Cu/SAPO-34 − Zeolite Acidity and Cu Structure Changes as a Function of Cu Loading. *Catal. Today* **2014**, *231*, 64−74.
(48) Bridgeman, A. J.; Gerloch, M. The Interpretation of Ligand Field Parameters. *Prog. Inorg. Chem.* **1997**, *45*, 180−281.
(49) Vanelderen, P.; Vancauwenbergh, J.; Tsai, M.-L.; Hadt, R. G.; Solomon, E. I.; Schoonheydt, R. A.; Sels, B. F. Spectroscopy and

Redox Chemistry of Copper in Mordenite. *ChemPhysChem* **2014**, *15*, 91−99.
(50) Schaffer, C. E. A Perturbation Representation of Weak Covalent Bonding. *Struct. Bonding (Berlin, Ger.)* **1968**, *5*, 68−95.
(51) Bendix, J. Ligfield. *Compr. Coord. Chem.* **2004**, *2*, 673−676.
(52) Piligkos, S.; Bendix, J.; Weihe, H.; Milios, C. J.; Brechin, E. K. A Ligand-Field Study of the Ground Spin-State Magnetic Anisotropy in a Family of Hexanuclear Mn(III) Single-Molecule Magnets. *Dalton. Trans.* **2008**, 2277−2284.
(53) Glerup, J.; Monsted, O.; Schaffer, C. E. Nonadditive and Additive Ligand Fields and Spectrochemical Series Arising from Ligand Field Parameterization Schemes. Pyridine as a Nonlinearly Ligating Pi-Back-Bonding Ligand toward Chromium(III). *Inorg. Chem.* **1976**, *15*, 1399−1407.
(54) Vennestrøm, P. N. R. Personal Communication, 2014.
(55) Jahn, H. A.; Teller, E. Stability of Polyatomic Molecules in Degenerate Electronic States. I. Orbital Degeneracy. *Proc. R. Soc. London A* **1937**, *161*, 220−235.
(56) Bersuker, I. B. *The Jahn-Teller Effect*; Cambridge University Press: New York, 2006.
(57) Öpik, U.; Pryce, M. H. L. Jahn-Teller Effect. I. A Survey of the Static Problem. *Proc. R. Soc. London A* **1957**, *238*, 425−447.
(58) Bates, S. A.; Verma, A. A.; Paolucci, C.; Parekh, A. A.; Anggara, T.; Yezerets, A.; Schneider, W. F.; Miller, J. T.; Delgass, W. N.; Ribeiro, F. H. Identification of the Active Cu Site in Standard Selective Catalytic Reduction with Ammonia on Cu-SSZ-13. *J. Catal.* **2014**, *312*, 87−97.